Have we found conclusive evidence for dark matter through direct detection experiments?

YANG Jun(杨俊)[1)]

Department of Physics, Shanghai Jiao Tong University, Shanghai 200240, China

Abstract: A WIMP-model-independent method is used to examine the existing evidence for low mass dark matter. Using XENON100's recent result of 224.6 live days × 34 kg exposure and PICASSO's result that was published in 2012, we have obtained constraints on the couplings $|a_{\rm n}|<0.4$ and $|a_{\rm p}|<0.3$, corresponding to spin-dependent cross-sections of $\sigma_{\rm n}<2.5\times10^{-38}$ cm^2 and $\sigma_{\rm p}<1.4\times10^{-38}$cm^2 for a WIMP mass of 10 GeV/c^2. It is shown that the spin-independent isospin-violating dark matter model also fails to reconcile the recent result from XENON100 with the positive results from DAMA, CoGeNT and CDMS-Ⅱ.

Key words: dark matter, spin-dependent, IVDM, XENOON100, direct detection

PACS: 95.35.+d, 14.80.Ly, 29.40.-n **DOI:** 10.1088/1674-1137/38/4/045101

1 Introduction

Since the term "dark matter" was first proposed by Fritz Zwicky in 1933 [1], a variety of astrophysical and cosmological observations have provided convincing evidence, indicating that something invisible but with great gravitational influence does in fact exist in our universe [2–5]. Now, it is generally accepted by astrophysicists that ordinary atomic matter makes a contribution of only 5% to the mass of the universe, while dark matter (DM) accounts for 23%, and the remaining 72% is dark energy [6]. Weakly Interacting Massive Particles (WIMPs), which are predicted by various extensions of the Standard Model, are believed to be the most suitable candidates for dark matter in the universe.

In light of WIMPs having weak or less-than-weak interactions with ordinary matter and the precondition, also supported by a recent observation [7], that the Milky Way is within a "dark halo", DM can be searched for directly on earth. The terrestrial experiments designed for DM direct detections are all based on these preconditions. The energy deposited on the target after each hit by a passing DM particle will be transferred to detectable signals, such as ionization, scintillation and phonons.

The two modes of WIMP-nucleon interaction, which the direct detectors are aiming at, are spin-independent (SI) and spin-dependent (SD). SI coupling, the scalar mode, describes coherent interactions of the entire nucleus with a WIMP. SD coupling, the axial mode, describes the interaction dependent on spin-content of the nucleus. Even though one of these experiments, DAMA/LIBRA, has been claiming success in finding DM signals for more than a decade [8, 9], other experiments only give a null result and thus have made exclusions in the cross-section and mass space for SI interaction [10–12]. Recent reports from CoGeNT [13], CRESST [14] and CDMS-Ⅱ [15] also show such evidence. A survey [16] presenting consistency for DAMA and CoGeNT's results in the low mass area (10–20 GeV/c^2) in the SI mode has drawn a great deal of attention. The survey applies the isospin-violating DM (IVDM) -nucleus interaction model, which assumes a different interaction strength between protons and neutrons; however, the analysis should be checked against XENON100's updated results [17].

In this article, a method of calculation for SI WIMP-nucleon scattering, focusing on the IVDM model, will be briefly introduced in Section 2. In Section 3 we focus on the SD interaction to show the up-to-date constraints for coupling constants at a WIMP mass of 10 GeV/c^2 by analysing several leading experiments. Following that, we present some discussion and conclusions in Section 4.

2 SI interactions

For elastic WIMP-nucleon scattering, the event rate of an Earth-bound detector can be written as [18]

$$R=N_{\rm T}\frac{\rho_{\rm D}}{M_{\rm D}}\int {\rm d}E_{\rm R}\int_{v_{\rm min}}^{v_{\rm esc}}\frac{{\rm d}\sigma}{{\rm d}E_{\rm R}}v\cdot f(\overrightarrow{v},\overrightarrow{v_{\rm E}}){\rm d}^3v, \qquad (1)$$

where $N_{\rm T}$ is the number of target nuclei, the local WIMP density $\rho_{\rm D}$=0.3 GeV/cm^3 [19], which when divided by

Received 21 February 2013, Revised 3 November 2013

1) E-mail: j.yang@sjtu.edu.cn

the WIMP mass, $M_{\rm D}$, denotes the local number density of WIMPs. The integral interval of recoil energy $E_{\rm R}$ is determined by experimental considerations. The lower limit of the velocity integral, $v_{\rm min}=\sqrt{M_{\rm A}E_{\rm R}/2\mu_{\rm A}^2}$, is the minimal value for a WIMP particle to deposit energy $E_{\rm R}$ on to a target atom, whose mass is $M_{\rm A}$, and $\mu_{\rm A}$ is the WIMP-nucleus reduced mass. The upper limit $v_{\rm esc}=544\pm64$ km/s [19] is the local Galactic escape velocity. A Maxwellian distribution, with characteristic velocity $v_0=220$ km/s [19], is assumed for $f(v)$, assuming for a staple dark halo model [18], where $\overrightarrow{v}$ is the DM velocity onto the detector while $\overrightarrow{v_{\rm E}}$ is the earth's velocity relative to the static galaxy.

The differential cross section, ${\rm d}\sigma/{\rm d}E_{\rm R}$, is model-dependent, and can be written in the general form,

$$\frac{{\rm d}\sigma}{{\rm d}E_{\rm R}}=\frac{\sigma_{\rm A}M_{\rm A}}{2v^2\mu_{\rm A}^2}F^2(q^2), \tag{2}$$

where the zero-momentum-transfer cross section $\sigma_{\rm A}$ and the form factor $F^2(q^2)$ are different for the two interaction modes.

In the SI model [20], the form factor proposed by Helm [21] is applicable to various sorts of targets, and the general form of the cross section can be written as

$$\sigma_{\rm A}^{\rm SI}=\frac{4}{\pi}\mu_{\rm A}^2[f_{\rm p}Z+f_{\rm n}(A-Z)]^2, \tag{3}$$

where $f_{\rm p}$ and $f_{\rm n}$ are the coupling constants for WIMP-proton and -neutron scattering, which is usually taken to be equal, $f_{\rm p}\approx f_{\rm n}=f$. Eq. (3) thus reduces to $\sigma_{\rm A}^{\rm SI}=(4f^2/\pi)\mu_{\rm A}^2A^2$, which is proportional to the square of the nucleon number A. However, the case where $f_{\rm p}\neq f_{\rm n}$ is called isospin-violating dark matter (IVDM). In Ref. [20], the assumption of a ratio, $f_{\rm n}/f_{\rm p}=-0.7$, has succeeded in breaking away from the constraints of XENON100 and reconciling CoGeNT with DAMA. Here, we apply the latest results from XENON100 with the same IVDM coupling to make an exclusion curve and check the region of agreement of CoGeNT with DAMA in Ref. [20]. We find that the once successful model fails the test this time, as shown in Fig. 1. Since XENON100 uses xenon as a target, which has seven isotopes, the value of $f_{\rm n}/f_{\rm p}=-0.7$ has reached its limit for reducing the constraints from the detector. It will no longer be able to invalidate the limit from XENON100.

CDMS-Ⅱ [15], which uses silicon as the target, has reported evidence that can survive the exclusion of XENON100's results for the IVDM condition. Nonetheless, it is not compatible with other evidence-found experiments. This is also shown in Fig. 1 for $f_{\rm n}/f_{\rm p}=-0.7$.

Obviously, the value of $f_{\rm n}/f_{\rm p}=-0.7$ is specific. A more general method for deciding the cross section (the coupling constants) for WIMP SI scattering provides an overall picture for a given WIMP mass, as shown in Fig. 2. The up-to-date $f_{\rm n}-f_{\rm p}$ region is constrained by

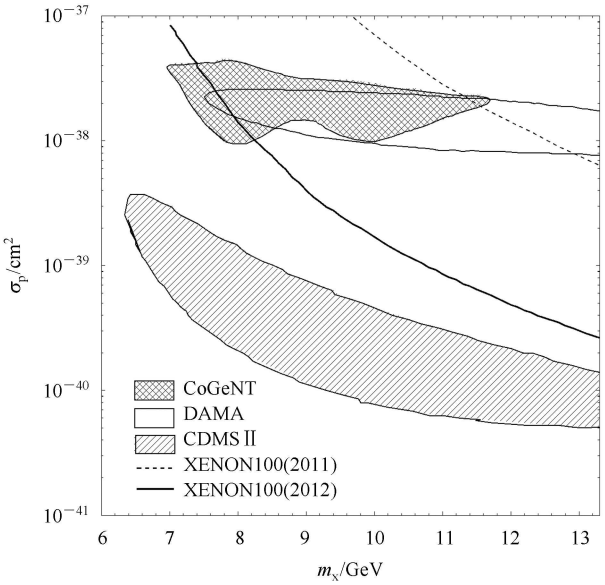

Fig. 1. For $f_{\rm n}/f_{\rm p}=-0.7$, the favored region of 90% CL bounds from CoGeNT and DAMA, from Ref. [20], are shown in grid hatching and unfilled contour, respectively. The exclusion curves from XENON100 are shown in dotted (for the 2011 result) and solid curves (for the 2012 result), respectively. The CDMS-Ⅱ evidence of 90% CL bounds for this coupling ratio, from Ref. [15], is shown in slant hatching.

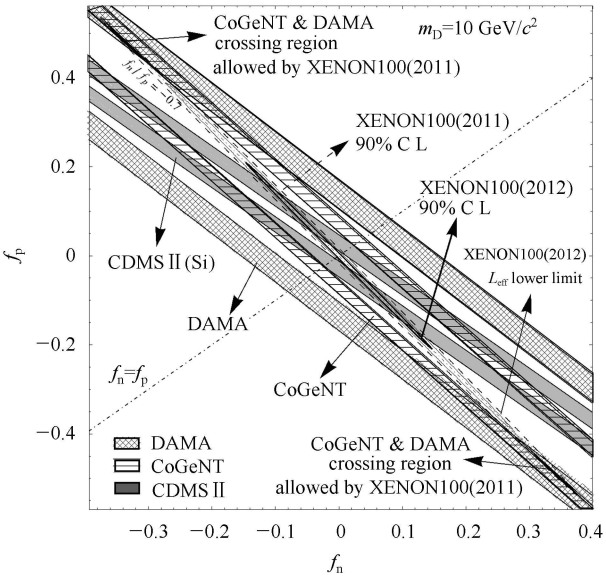

Fig. 2. SI couplings for a 10 GeV/c^2 WIMP.

XENON100's recent result, which is shown as the inner section of the orange ellipse.

In Fig. 2, the allowed area of the coupling constants $f_{\rm p}$ and $f_{\rm n}$ is the inner region of the ellipses. The filled bands represent the CoGeNT, DAMA and CDMS-Ⅱ evidence. Although XENON100's 2011 results, the

dashed ellipse, have left some room for the evidence from CoGeNT and DAMA (filled in black), the recent XENON100 results, shown by the bold solid ellipse, have thoroughly excluded it. The fine black ellipse, which takes the lower limit of light efficiency [22] into consideration, rules out the scintillation uncertainties of XENON from changing this excluded result. CDMS-Ⅱ's reported evidence [15] can survive in a large area of the allowed coupling region. However, from Fig. 2, we can see that no common area exists for the evidence of all three experiments (DAMA filled with grid, CoGeNT filled with line and CDMS-Ⅱ in gray) allowed by XENON100. There is, therefore, an inconsistency in the results from these experiments.

3 SD interactions

For Majorana fermions, which do not have vector interactions, only two cases need to be considered: the scalar interaction (SI mode), which has been introduced in Section 2, and the spin-spin interaction (SD mode). In the case of SD interaction, the estimation of WIMP-nucleus interactions is done firstly by calculating the WIMP-quark and WIMP-gluon interaction. Then, the WIMP-nucleon and finally the WIMP-nucleus interaction can be calculated. However, in the first step of the process, the couplings of WIMPs with quarks and gluons are WIMP-model-dependent, as are the masses of the exchanged particles and some other important quantities. WIMP-nucleon scattering cross sections have a considerable dependence on a particular WIMP type. Thus, it is preferable to use a WIMP-model-independent method [23] to do the survey.

The general form of a SD cross section is given as [24]

$$\sigma_{\rm A}^{\rm SD}(q)=\frac{32G_{\rm F}^2\mu_{\rm A}^2}{2J+1}S(q), \tag{4}$$

where $G_{\rm F}$ is the Fermi constant and $\mu_{\rm A}$ is the nucleus-WIMP reduced matter. When normalized, $S(q)/S(0)$ is the form factor for the SD mode, which is the counterpart of $F^2(q^2)$ in the SI mode. The expression of $S(q)$ can be expanded to

$$S(q)=[a_{\rm p}^2S_{\rm pp}(q)+a_{\rm p}a_{\rm n}S_{\rm pn}(q)+a_{\rm n}^2S_{\rm nn}(q)], \tag{5}$$

$$\begin{aligned} S_{\rm pp} &= S_{00}(q)+S_{01}(q)+S_{11}(q),\\ S_{\rm nn} &= S_{00}(q)-S_{01}(q)+S_{11}(q),\\ S_{\rm pn} &= 2[S_{00}(q)-S_{11}(q)], \end{aligned} \tag{6}$$

where $S_{\rm i,j}$ (i,j=p,n) is the spin structure, which is specific to each nucleus. The coupling constants are denoted as $a_{\rm p}$ and $a_{\rm n}$. In the case of zero momentum transfer,

$$S(0)=\frac{2J+1}{\pi}\lambda^2J(J+1), \tag{7}$$

where λ is given in the form [25],

$$\lambda=\frac{\langle N|(a_{\rm p}S_{\rm p}+a_{\rm n}S_{\rm n})|N\rangle}{\left\langle N\middle|\hat{J}\middle|N\right\rangle}=\frac{1}{J}(a_{\rm p}\langle S_{\rm p}\rangle+a_{\rm n}\langle S_{\rm n}\rangle). \tag{8}$$

From Eqs. (4), (7), (8), the zero momentum cross section for SD is then

$$\sigma_{\rm A}^{\rm SD}=\frac{32}{\pi}G_{\rm F}^2\mu_{\rm A}^2[a_{\rm p}\langle S_{\rm p}\rangle+a_{\rm n}\langle S_{\rm n}\rangle]^2\frac{J+1}{J}, \tag{9}$$

where $\langle S_{\rm p}\rangle$ and $\langle S_{\rm n}\rangle$ are the spin expectations for proton and neutron, respectively, in the odd-group nuclear model, and J is the total nuclear angular momentum. For a single nucleon whose spin and total angular momentum are of the same value 1/2,

$$\sigma_{\rm p,n}=\frac{24}{\pi}G_{\rm F}^2\mu_{\rm p}^2a_{\rm p,n}^2. \tag{10}$$

Neglecting the small difference between $\mu_{\rm n}$ and $\mu_{\rm p}$, we can rewrite Eq. (9) using Eq. (10)

$$\sigma_{\rm A}^{\rm SD}=\frac{4}{3}\frac{\mu_{\rm A}^2}{\mu_{\rm p}^2}\left(\langle S_{\rm p}\rangle\sqrt{\sigma_{\rm p}}+\langle S_{\rm n}\rangle\sqrt{\sigma_{\rm n}}\right)^2\frac{J+1}{J}. \tag{11}$$

For simplicity, when calculating the contour of WIMP-proton (neutron) cross section versus WIMP mass, experiments [26–28] sometimes adopt the method of setting $a_{\rm n}$ ($a_{\rm p}$) to zero. Then

$$\begin{aligned} \sigma_{\rm A}^{\rm p}&=\frac{32}{\pi}G_{\rm F}^2\mu_{\rm A}^2(a_{\rm p}\langle S_{\rm p}\rangle)^2\frac{J+1}{J},\\ \sigma_{\rm A}^{\rm n}&=\frac{32}{\pi}G_{\rm F}^2\mu_{\rm A}^2(a_{\rm n}\langle S_{\rm n}\rangle)^2\frac{J+1}{J}. \end{aligned} \tag{12}$$

The SD cross section can then be rewritten as

$$\sigma_{\rm A}=(\sqrt{\sigma_{\rm A}^{\rm p}}\pm\sqrt{\sigma_{\rm A}^{\rm n}})^2. \tag{13}$$

The sign in Eq. (13) is identical to the sign of $\langle S_{\rm p}\rangle/\langle S_{\rm n}\rangle$. Comparing Eq. (10) and Eq. (12) then gives

$$\sigma_{\rm n,p}=\frac{1}{\langle S_{\rm n,p}\rangle^2}\frac{J}{J+1}\frac{3}{4}\frac{\mu_{\rm p}^2}{\mu_{\rm A}^2}\sigma_{\rm A}^{\rm n,p}. \tag{14}$$

So far, we have used a common method for making contours or drawing exclusion curves from experimental data. However, this assumes a specific WIMP model by setting $a_{\rm p}$ or $a_{\rm n}$ to zero.

A more general way is to use Eq. (9) as a model-independent calculation without assuming a certain value for $a_{\rm p,n}$. Actually, the value of $a_{\rm p}=0$ and $a_{\rm n}=0$ are two special points on the $a_{\rm p}-a_{\rm n}$ contour. This is clear after the integration of Eq. (1), combining Eqs. (2), (4), (9). The outcome has the form of

$$N=Aa_{\rm p}^2+Ba_{\rm p}a_{\rm n}+Ca_{\rm n}^2, \tag{15}$$

Eq. (15) is a conic section. If $B^2<4AC$ then it is an ellipse whose center is the origin and $(a_{\rm n},0)$, $(0,a_{\rm p})$ are two points of intersection with the axes. Otherwise, it is one of two open curves: a hyperbola when $B^2>4AC$, or two

parallel lines if $B=\pm 2\sqrt{AC}$. When the target only contains a single nucleon that is sensitive to SD interaction, Eq. (15) changes to

$$N'=(A'a_{\rm p}+C'a_{\rm n})^2, \tag{16}$$

which shows that the ellipse has degenerated into two parallel lines. In this calculation, PICASSO's [29] target has a single isotope of fluorine that is $a_{\rm p}$ sensitive. CoGeNT's [13] target has ^{73}Ge which is the only $a_{\rm n}$-sensitive isotope among all the natural isotopes of germanium. Thus, the calculation results of these two experiments are both two parallel lines in the $a_{\rm p}-a_{\rm n}$ coordinate. DAMA [30] uses a NaI target, of which both elements have good sensitivity for SD interactions. However, in the low WIMP mass area around 10 GeV/c^2, the scattering does not deposit enough energy to reach the threshold level for iodine, so only sodium, which has a single nature isotope, works. This means that the region allowed by DAMA is between two parallel lines but is not an ellipse for a WIMP mass of 10 GeV/c^2. For XENON100, two out of the seven isotopes of its target are sensitive to SD scattering, and thus it comes out as an ellipse.

The XENON100 experiment uses targets with an isotope abundance of 26.2% for ^{129}Xe and 21.8% for ^{131}Xe, both of which are sensitive to WIMP-neutron SD scattering. The results show that two candidate events have been observed in the energy range 6.6–30.5 keV$_{\rm nr}$ from 224.6 live days $\times$34 kg exposure[17]. In the analysis, an energy range of 6.6–43.3 keV$_{\rm nr}$ (3–30PE) is used with the expected background of 1.0±0.2. Applying the Feldman-Cousins procedure [31], we obtain the current strongest limit for $a_{\rm n}$. In the calculation, we apply the spin structure from Menendez, Gazit and Schwenk's work (MGS for short) [32], and another work by Ressell and Dean (RD) [33] is taken for reference.

For CoGeNT and DAMA, we calculate at the mass point of 10 GeV/c^2 to find the region of agreement in the $\sigma_{\rm p}-\sigma_{\rm n}$ area. When dealing with GoGeNT's results [16], the calculation is done by integrating Eq.(1) using the cross section form shown in Eq. (9). An alternative way [23], shown in Eq. (17), is applied to the calculation for DAMA [8] since only ^{23}Na produces detectable signals at this WIMP mass point (see Appendix A)

$$\sum_{A_i}\left(\frac{a_{\rm p}}{\sqrt{\sigma_{\rm p}^{\lim(A_i)}}}\pm\frac{a_{\rm n}}{\sqrt{\sigma_{\rm n}^{\lim(A_i)}}}\right)^2=\frac{\pi}{24G_{\rm F}^2\mu_{\rm p}^2}, \tag{17}$$

where $\sigma_{\rm p,n}^{\lim(A_i)}$ is the nucleon cross section, accounting for the total event rate.

We take PICASSO's [28, 29] result for the $a_{\rm p}$ constraint because its low threshold energy qualifies it to provide a test in the low mass (10 GeV/c^2) region. The experiment use superheated C_4F_{10}, with a droplet of the target exploding into a vapor bubble after being hit by a WIMP. In virtue of its single nuclear interaction in SD mode, we can easily obtain $\sigma_{\rm n}^{\lim A}$ from the published $\sigma_{\rm p}^{\lim A}$ by

$$\frac{\sigma_{\rm p}^{\lim A}}{\sigma_{\rm n}^{\lim A}}=\frac{\langle S_{\rm n}\rangle^2}{\langle S_{\rm p}\rangle^2}. \tag{18}$$

The spin expectation is listed in Table 1.

In dealing with CoGeNT's spectrum [16], we adopt the most stringent surface event rejection to check the lower limit of its couplings (cross-sections) with a 99% confidence level. If even the most stringent surface event rejection region is excluded, other coupling regions under a milder surface rejection will also be excluded.

In Fig. 3, the allowed region for $a_{\rm p}$ and $a_{\rm n}$ is constrained both by XENON100's ellipse and PICASSO's parallel lines(dotted lines for 2011's result and solid lines for 2012's result), which is filled in black under the constraint of XENON100(2012)'s result [17] (inclined ellipse) and PICASSO(2012)'s result [29] (solid lines).

Table 1. Spin values for relevant nuclides.

nucleus	odd	J	$\langle S_{\rm p}\rangle$	$\langle S_{\rm n}\rangle$	Ref.
^{19}F	p	1/2	0.441	−0.109	[34]
^{23}Na	p	3/2	0.248	0.020	[33]
^{73}Ge	n	9/2	0.030	0.378	[35]
^{129}Xe	n	1/2	0.010	0.329	[32]
^{131}Xe	n	3/2	−0.009	−0.272	[32]

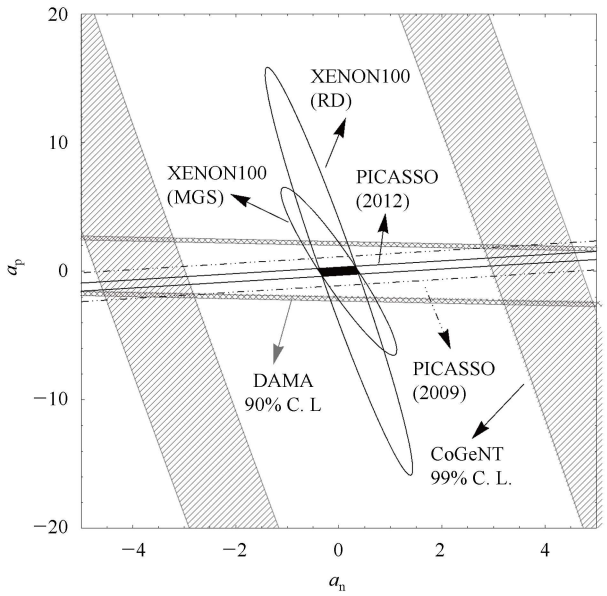

Fig. 3. SD couplings allowed by XENON100 (black ellipse) and PICASSO (solid lines for 2012's result) at a WIMP mass of 10 GeV/c^2 (filled in black). The regions allowed by DAMA (grid hatching) and CoGeNT (slant hatching) have been ruled out.

CoGeNT and DAMA's evidence (slant and grid hatching) is clearly excluded.

4 Discussion and conclusions

In this article, we have examined the signal reported by the DAMA/NaI, CoGeNT and CDMS-Ⅱ experiments, compared with the recent results from the XENON100 and PICASSO experiments. The 10 GeV/c^2 DM evidence is excluded for the SD model. For SI interactions, the IVDM model also fails to keep the signal from DAMA and CoGeNT's from being excluded. CDMS-Ⅱ has reported an excess of nuclear recoil events above their estimated background. So far, these signal cannot be ruled out by other experiments in the IVDM model. However, it is not yet clear whether these signals are from WIMPs or from an unknown background. There is a lack of agreement in the leading experiments' results.

1) The IVDM model with $f_{\rm n}/f_{\rm p}=-0.7$ is unable to keep the compatible region from CoGeNT and DAMA from being excluded by the constraints from XENON100. There is no agreement in the results from CDMS-Ⅱ, GoGeNT and DAMA. That is to say, in SI mode, there is no positive evidence from DM direct detection experiments.

2) Within the constraints from XENON100 (2012) and PICASSO (2012), for a 10 GeV/c^2 DM mass, we have obtained the allowed coupling regions of $|a_{\rm n}|<0.4$ and $|a_{\rm p}|<0.3$, corresponding to the cross-sections $\sigma_{\rm n}<2.5\times10^{-38}$ cm^2 and $\sigma_{\rm p}<1.4\times10^{-38}$ cm^2. Thus, in SD mode, no WIMP signal is compatible within all of the experimental results.

For the SD calculation, a model-independent method has been introduced. While experiments usually report the cross-section for pure neutron or pure proton channels, this is insufficient to give a full comparison between different detectors. This has been done in Section 3 for a 10 Gev/c^2 WIMP. Other masses are also excluded using the same method.

The author would like to thank Mr. K. Ni for useful discussion and helpful advice given on the improvement of this work.

Appendix A

Derivation of Eq. (17) in section 3

For a multiple-nucleus target, Eq. (17) offers a simplified method to obtain the region of allowed coupling constants if the nuclear cross section reported is obtained by the procedure that accounts for the total event rate for each isotope.

In detail, after combining Eqs. (1), (2), (9), the integration is in the form

$$\begin{aligned} R &= \sum_{A_i} N_{\rm T}\frac{\rho_{\rm D}}{M_{\rm D}}\int {\rm d}E_{\rm R}\int_{v_{\rm min}}^{v_{\rm esc}} {\rm d}^3v f(v)\frac{\sigma^0_{\rm SD}M_{A_i}}{2v\mu^2_{A_i}}F^2_{A_i}(q^2) \\ &= \sum_{A_i} C_{A_i}\frac{32}{\pi}G^2_{\rm F}\mu^2_{A_i}[a_{\rm p}\langle S_{\rm p}\rangle+a_{\rm n}\langle S_{\rm n}\rangle]^2\frac{J+1}{J}, \end{aligned} \tag{A1}$$

where A_i denotes the $i^{\rm th}$ nucleus. C_{A_i} is the constant for the $i^{\rm th}$ nucleus derived after integration over velocity and recoil energy.

If experiments account for the total event rate for each single isotope, that is $\sigma^{\rm n,p}_{A_j}=\sigma^0_{\rm SD}$, then

$$\begin{aligned} R &= N_{\rm T}\frac{\rho_{\rm D}}{M_{\rm D}}\int {\rm d}E_{\rm R}\int_{v_{\rm min}}^{v_{\rm esc}} {\rm d}^3v f(v)\frac{\sigma^0_{\rm SD}M_{A_j}}{2v\mu^2_{A_j}}F^2_{A_j}(q^2) \\ &= C_{A_j}\sigma^{n,p}_{A_j}, \end{aligned} \tag{A2}$$

where A_j is the $j^{\rm th}$ arbitrary target nucleus.

Comparing Eq. (A1) with Eq. (A2), we obtain

$$\sum_{A_i}\frac{C_{A_i}}{C_{A_j}}\frac{32}{\pi}G^2_F\mu^2_{A_i}\left[\frac{a_{\rm p}\langle S_{\rm p}\rangle}{\sqrt{\sigma^{\rm p}_{A_j}}}+\frac{a_{\rm n}\langle S_{\rm n}\rangle}{\sqrt{\sigma^{\rm n}_{A_j}}}\right]^2\frac{J+1}{J}=1. \tag{A3}$$

For each $j=i$ and with Eq. (14):

$$\sigma_{\rm n,p}=\frac{1}{\langle S_{\rm n,p}\rangle^2}\frac{J}{J+1}\frac{3}{4}\frac{\mu^2_{\rm p}}{\mu^2_{\rm A}}\sigma^{\rm n,p}_{\rm A}. \tag{A4}$$

We thus derive Eq. (17)

$$\sum_{A_i}\left(\frac{a_{\rm p}}{\sqrt{\sigma^{\lim(A_i)}_{\rm p}}}\pm\frac{a_{\rm n}}{\sqrt{\sigma^{\lim(A_i)}_{\rm n}}}\right)^2=\frac{\pi}{24G^2_{\rm F}\mu^2_{\rm p}}. \tag{A5}$$

It can be seen from the derivation that Eq. (17) can be used appropriately when $\sigma^{\lim(A_i)}_{\rm p,n}$ accounts for the total event rate. It will not be correct when the reported WIMP-nucleon cross section is derived from a mixed nucleus calculation.

References

1 Zwicky F. Astrophys. J, 1937, **86**: 217
2 Babcock H W. Lick Observatory Bulletin, 1939, **19**: 41
3 Rubin V C, Ford W K J. Astrophys. J, 1970, **159**: 379
4 Roberts M S, Whitehurst R N. Astrophys. J, 1975, **201**: 327
5 Jee M J et al. Astrophys. J, 2007, **661**: 728
6 Komatsu E et al. (WMAP collaboration). Astrophys. J. Suppl., 2011, **192**: 18
7 Garbari S et al. MNRAS, 2012, **425(2)**: 1445
8 Savage C et al. JCAP, 2009, **0904**: 010
9 Bernabei R, Belli P, Cappella F et al. Eur. Phys. J. C, 2010 **67**: 39
10 Ahmed Z et al. (CDMS). Phys. Rev. Lett., 2011, **106**: 131302
11 Angle J et al. (XENON10). Phys. Rev. Lett., 2011, **107**: 051301
12 Armengaud E et al. (EDELWEISS). Phys. Rev. D, 2012, **86**: 051701
13 Aalseth C E et al. (CoGeNT). Phys. Rev. Lett., 2011, **107**: 141301
14 Angloher G et al. (CRESST-Ⅱ). Eur. Phys. J. C, 2012, **72**: 1971
15 Kahlhoefer F et al. arXiv:1304.6066
16 Kelso C, Hooper D, Buckley M R. Phys. Rev. D, 2012, **85**: 043515
17 Aprile E et al. (XENON100). Phys. Rev. Lett., 2012, **109**: 181301
18 Lewin J D, Smith P F. Astropart. Phys, 1996, **6**: 87
19 Smith M C et al. Mon. Not. R. Astron. Soc, 2007, **379**: 755
20 Feng J L et al. Phys. Lett. B, 2011, **703**: 124
21 Helm R H. Phys. Rev., 1956, **104**: 1466
22 Plante G, Aprile E et al. Phys. Rev. C, 2011, **84**: 045805
23 Tovey D R et al. Phys. Lett. B, 2000, **488**: 17
24 Savage C, Gondolo P, Freese K. Phys. Rev. D, 2004, **70**: 123513
25 Engel J, Vogel P. Phys. Rev. D, 1989, **40**: 3132
26 Felizardo M, Girard T A et al. Phys. Rev. Lett., 2012, **108**: 201302
27 Lebedenko V N et al. Phys. Rev. Lett., 2009, **103**: 151302
28 Archambault S et al. Phys. Lett. B, 2009, **682**: 185
29 Archambault S et al. Phys. Lett. B, 2012, **711**: 153
30 Savage C, Gondolo P, Freese K. Phys. Rev. D, 2004, **70**: 123513
31 Feldman G J, Cousins R D. Phys. Rev. D, 1998, **57**: 3873
32 Menendez J, Gazit D, Schwenk A. Phys. Rev. D, 2012, **86**: 103511
33 Ressell M T, Dean D J. Phys. Rev. C, 1997, **56**: 535
34 Pacheco A F, Strottman D D. Phys. Rev. D, 1989, **40**: 2131
35 Jungman G, Kamionkowski M, Griest K. Phys. Rep., 1996, **267**: 195